RSC Advances

PAPER

View Article Online
View Journal | View Issue

Cite this: *RSC Adv.*, 2020, **10**, 6822

The influence of hydrogen concentration in amorphous carbon films on mechanical properties and fluorine penetration: a density functional theory and *ab initio* molecular dynamics study†

Hwanyeol Park,[ab] Daekwang Woo,[b] Jong Myeong Lee,[b] Se Jun Park,[b] Sungwoo Lee,[a] Ho Jun Kim,[c] Euijoon Yoon*[ad] and Gun-Do Lee*[ad]

Amorphous carbon (a-C) films have attracted significant attention due to their reliable structures and superior mechanical, chemical and electronic properties, making them a strong candidate as an etch hard mask material for the fabrication of future integrated semiconductor devices. Density functional theory (DFT) calculations and *ab initio* molecular dynamics (AIMD) simulations were performed to investigate the energetics, structure, and mechanical properties of the a-C films with an increasing sp^3 content by adjusting the atomic density or hydrogen content. A drastic increase in the bulk modulus is observed by increasing the atomic density of the a-C films, which suggests that it would be difficult for the films hardened by high atomic density to relieve the stress of the individual layers within the overall stack in integrated semiconductor devices. However, the addition of hydrogen into the a-C films has little effect on increasing the bulk modulus even though the sp^3 content increases. For the F blocking nature, the change in the sp^3 content by both atomic density and H concentration makes the diffusion barrier against the F atom even higher and suppresses the F diffusion, indicating that the F atom would follow the diffusion path passing through the sp^2 carbon and not the sp^3 carbon due to the significantly high barrier. For the material design of a-C films with adequate doped characteristics, our results can provide a new straightforward strategy to tailor the a-C films with excellent mechanical and other novel physical and chemical properties.

Received 10th November 2019
Accepted 30th January 2020

DOI: 10.1039/c9ra09328a

rsc.li/rsc-advances

1. Introduction

Amorphous carbon (a-C) films have attracted significant attention due to their reliable structures and superior mechanical, chemical and electronic properties,[1–3] making them a strong candidate as an etch hard mask material for the fabrication of future integrated semiconductor devices. However, for wider applications, it is still necessary to overcome the current limitations such as high internal stresses, low blocking nature of fluorine attack to sub-layers, and low temperature stability.[4] In order to eliminate the aforementioned drawbacks and enhance the properties of the a-C films, the influence of hydrogen to modify their structure during the deposition process was studied.

The a-C films are mainly deposited on large areas at relatively low temperatures by plasma-enhanced chemical vapor deposition (PECVD) using hydro-carbon mixed precursor gases such as CH_4 or C_2H_2 diluted in H_2.[5,6] However, it is well known that the F atoms, which originate from the injection of etchant gases such as CF_x during the device fabrication process, generally attack the sub-layers and significantly degrade the device performance due to the extremely high reactive nature of F atoms with other atoms that have an electron-donating nature such as B, Al, and Ga; this results in the bond breaking of sub-layer materials to form F-containing alloys. This problem is a primary obstacle in the development of future integrated semiconductor devices.[7,8] To address this problem, a theoretical comprehension of the a-C films is required for the device fabrication process due to the experimentally limited observations on the atomistic scale.

The properties of the a-C films depend on the sp^3-to-sp^2 hybridization ratio and the H content.[9,10] Depending on the composition, these films exhibit different characteristics such as hardness, electrical resistivity, optical transparency, and

[a]*Department of Materials Science and Engineering, Seoul National University, Seoul 08826, Korea. E-mail: eyoon@snu.ac.kr; gdlee@snu.ac.kr*

[b]*Memory Thin Film Technology Team, Giheung Hwaseong Complex, Samsung Electronics, 445-701, South Korea*

[c]*Department of Mechanical Engineering, Dong-A University, Busan 49315, South Korea*

[d]*Research Institute of Advanced Materials, Inter-university Semiconductor Research Center, Seoul National University, Seoul 08826, South Korea*

† Electronic supplementary information (ESI) available. See DOI: 10.1039/c9ra09328a

chemical inertness. The a-C films with high hardness, high sp^2 content, and low optical band gaps are referred to as hard graphitic a-C.[11] On the other hand, the a-C films with hardness and resistivity similar to that of a diamond are referred to as diamond-like carbon (DLC).[12]

Briefly, in previous studies, Mikami *et al.*[13] found that an increase in the H_2 flow rate leads to an increase in the sp^3 fraction and disorder during the deposition of the DLC films by radiofrequency (RF) magnetron sputtering. Vietzke *et al.*[14] investigated the hydrogen-induced chemical erosion of C atoms from the a-C films using mass spectrometry. They reported the formation of CH_3 radicals along with a wide range of high hydrocarbons due to the reaction of the thermal H atoms within the a-C films. Other researchers reported that the growth rate, film structure, mechanical properties, optical gaps and field emission were all considerably affected by hydrogen.[15,16]

Although several experimental studies on the influence of the hydrogen content in an a-C film have been investigated, no guidelines exist for improving the a-C film as an etch hard mask because the relationship between the structure of the a-C film and its etching characteristics remains unclear. *Ab initio* calculations provide a powerful tool to determine the atomic and electronic details and provide a deeper insight into the stress reduction mechanism of the a-C films.[17–19]

In this paper, we examine the energetics, structure, and mechanical properties of a-C films with increasing sp^3 content by adjusting the atomic density or hydrogen content using density functional theory (DFT) and *ab initio* molecular dynamics (AIMD) calculations. In our simulation, we generated amorphous carbon structures containing 64 C atoms to focus on studying the influence of the increase in the sp^3 content by adjusting the atomic density or hydrogen content on the mechanical properties during the device fabrication processes.

We also theoretically investigated the influence of the increase in the sp^3 content by adjusting the atomic density or hydrogen content on the diffusion of F atoms during the dry etch process, generating important findings in the field of materials science.

2. Computational methods

2.1. Generation of the model structure

Ab initio molecular dynamics (AIMD) simulations were carried out to obtain amorphous carbon structures. The cubic supercell of 64 atoms with a fixed lattice constant of 7.61 Å was used, which corresponded to the density of the reference amorphous carbon with 2.9 g cm^{-3}.

The melt-quench simulations[20,21] were performed by pre-melting for 2 ps at 12 000 K, melting for 10 ps at 5000 K, and quenching to 0 K with a constant cooling rate of -250 K ps^{-1}. In the designed doped amorphous structures, the densities of dense a-C structures were selected as 3.2, 3.5, and 4.0 g cm^{-3}, which corresponded to the lattice constants of 7.36, 7.14, and 6.83 Å. Hydrogen concentrations in H-added a-C structures were selected as 15.6, 23.4, and 31.2 at%, corresponding to 10, 15, and 20 atoms in 64-atom models. The final amorphous carbon structure was obtained by full relaxation of the atomic positions. Finally, the amorphous carbon structure comprised a tetra-coordinated C fraction of 56.3% with a radius of 1.8 Å to define the distances between the nearest neighbours for all amorphous carbon structures. This cut-off radius was obtained by calculating the first minimum value in the radial distribution function (RDF).[22]

2.2. DFT calculations

In our theoretical results, all DFT calculations were performed using the Vienna *Ab initio* Simulation Package (VASP) program with the Perdew–Burke–Ernzerhof (PBE) functional in the generalized gradient approximation (GGA).[23,24] We used the PBE-D2 functional[25] based on the projector augmented wave (PAW) method[26] with a conventional Kohn–Sham DFT energy correction to treat the van der Waals interactions for all DFT calculations (see the ESI†[27]).

Valence orbitals were described by a plane-wave basis set with the cut-off energy of 400 eV. Ultrasoft Vanderbilt-type pseudopotentials[28] were used to describe the interactions between ions and electrons. The Brillouin zone for all amorphous structures was sampled with a $3 \times 3 \times 3$ Monkhorst–Pack *k*-point mesh. Geometry optimization was performed by minimizing the forces of all atoms to less than 0.02 eV $Å^{-1}$ with the total energy of the system converged within 10^{-4} eV during self-consistent iterations. We determined the energy barriers (activation energies) through the climbing-image nudged elastic band (CINEB) method[29] using a force tolerance of 0.02 eV $Å^{-1}$. For an accurate calculation of the barriers, the CINEB method with a more precise transition-state search algorithm than the NEB method was used.[30,31] This method was made to search one of the various states near the transition-state along the reaction path, converging at the highest saddle point.[32–35]

3. Results and discussion

3.1. Influence of atomic density and hydrogen concentration on mechanical properties

Fig. 1 shows the final atomic structures of 64 C atom-containing a-C films with an increase in the atomic density (3.2 to 4.0 g cm^{-3}) and hydrogen concentrations (15.6 to 31.2 at%). The dependence of the calculated bulk modulus on the atomic density is illustrated in Fig. 2(a). In the case of the reference a-C film (Ref. a-C), a bulk modulus of about 212 GPa was estimated. With the increase in atomic density, the bulk modulus drastically increased; when the atomic density was 4.0 g cm^{-3}, a maximal bulk modulus of about 617 GPa was obtained, which was around three-fold larger than that of the reference a-C film. On the other hand, on introducing H atoms in the a-C films, as shown in Fig. 2(b), the bulk modulus as a function of the H concentration increased and then slightly increased. When the H concentration was 31.2 at%, a maximal bulk modulus of about 248 GPa was obtained, which slightly increased by 17% compared to that for the reference a-C film.

I. N. Remediakis *et al.*,[36] revealed that the bulk modulus of a-C films was enhanced as the film density increased (335 GPa at 2.7 g cm^{-3}, 375 GPa at 3.05 g cm^{-3}, and 465 GPa at 3.55 g cm^{-3}).

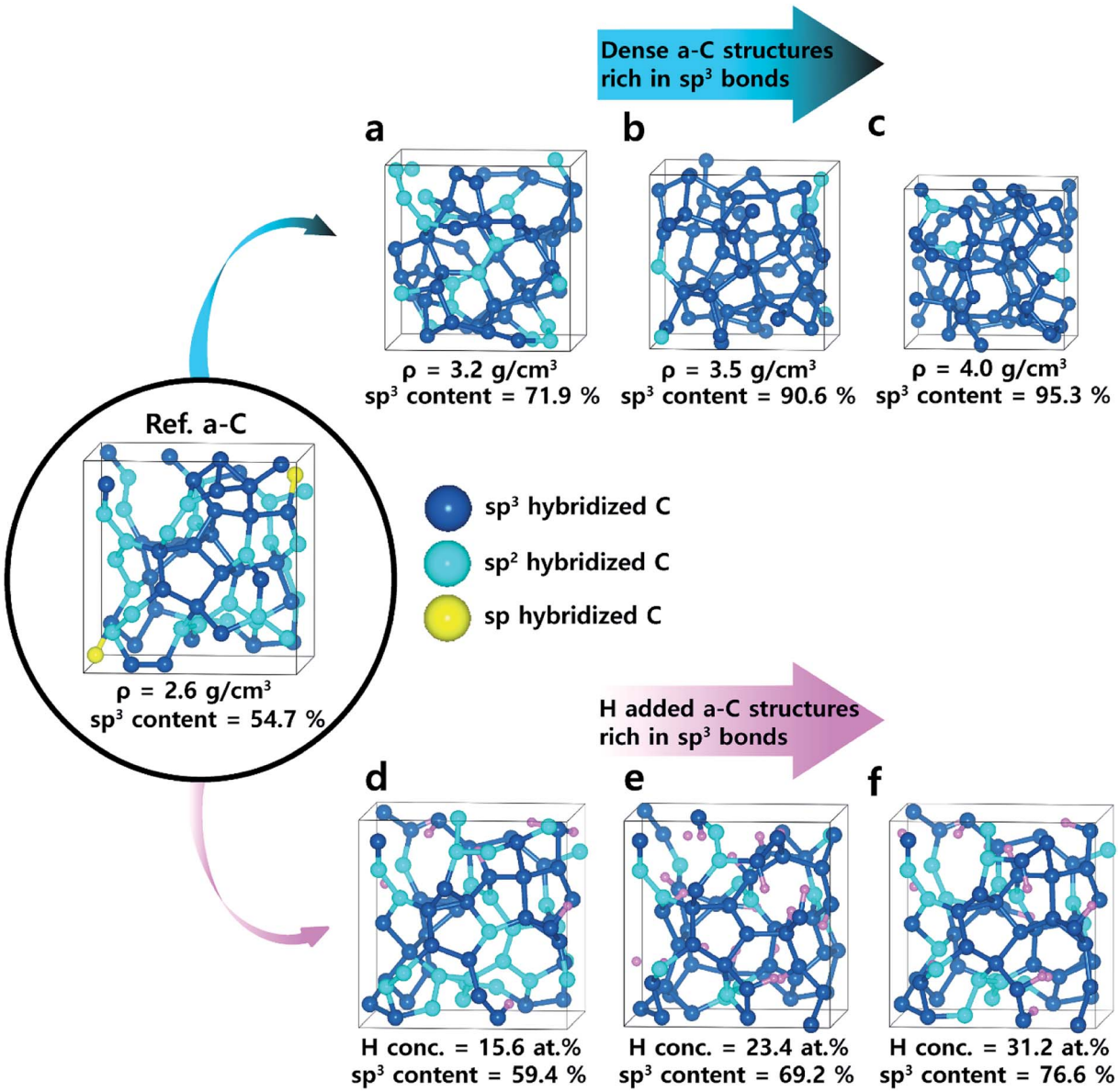

Fig. 1 Optimized atomic structures of 64 C atom-containing amorphous carbon structures with increasing atomic density (3.2 to 4.0 g cm^{-3}) and hydrogen concentrations (15.6 to 31.2 at%). Blue, sky-blue, yellow, and pink colors indicate sp^3, sp^2, sp hybridized C and H atoms, respectively.

This experimental result showed a similar trend with our DFT results (212 GPa at 2.6 g cm^{-3}, 351 GPa at 3.2 g cm^{-3}, and 450 GPa at 3.5 g cm^{-3}); however, there is some discrepancy since the amorphous phase is characterized by a short-range order and the atoms are bonded in randomly disordered positions due to a phenomenon that does not allow the formation of a regular arrangement.

Nevertheless, taking advantage of the benefits of the simulation, it is noted that the drastic increase in the bulk modulus is observed by increasing the atomic density of the a-C films, which suggests that it would be difficult for the films hardened by high atomic density to relieve the stress of the individual layers within the overall stack in integrated semiconductor devices. However, the addition of hydrogen in the a-C films has little effect on increasing the bulk modulus even though the sp^3 content increases. These findings suggest that the process design for high-sp^3-content a-C films should be carried out by adding hydrogen rather than increasing the atomic density. These requirements become more important and increasingly challenging to meet as the device integrity increases.[37,38] To elucidate the mechanism of the increase in bulk modulus caused by atomic density and hydrogen concentrations, more direct evidence for the atomic bond structure including bond length distributions was collected first.

Fig. 3 shows the calculated results of the bond length and bond angle distributions for the dense a-C film with the highest atomic density of 4.0 g cm^{-3} and those for the H-added a-C film with the highest H concentration of 31.2 at%, in which the

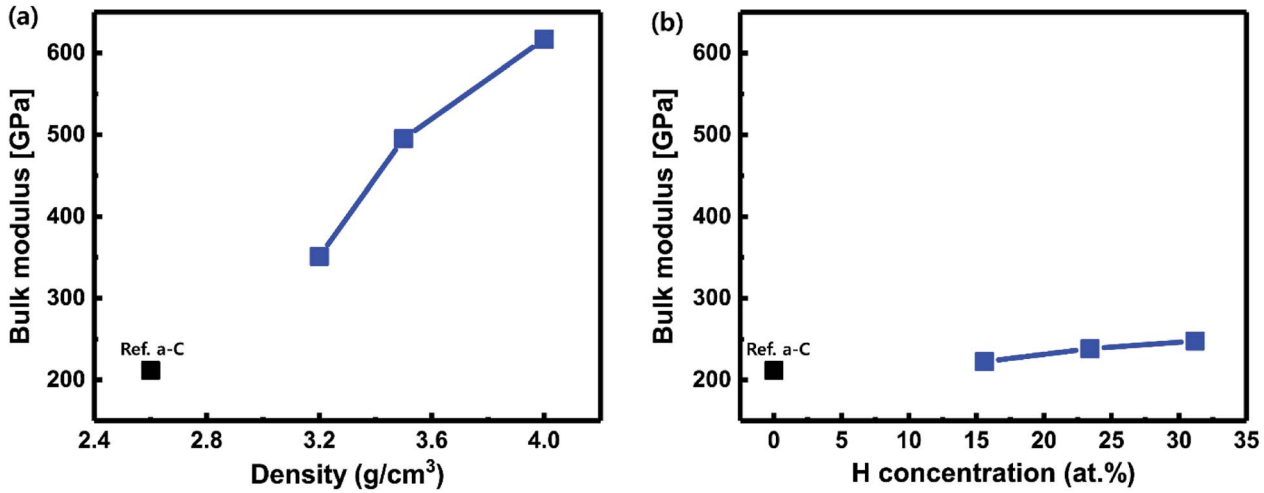

Fig. 2 Dependency of the calculated bulk modulus on (a) atomic density from 3.2 to 4.0 g cm^{-3} and (b) hydrogen concentrations from 15.6 to 31.2 at%, corresponding to 10 H, 15 H, and 20 H-added a-C.

highest bulk modulus is observed, as shown in Fig. 2. For comparison, the case for the Ref. a-C film was also considered. The total bond length and bond angle distributions shown in Fig. 3 mainly consist of a C–C bond. Li *et al.*[39] revealed that the distortion of bond lengths (<1.42 Å) and bond angles (>120°) in the carbon network was the key factor for the low level of the bulk modulus. Therefore, the bond lengths and bond angles in these three a-C films were particularly studied in order to gain the fractions of distorted bonds, which are illustrated in Table 1. The equilibrium bond lengths of stable sp^2 and sp^3 C–C bonds are 1.42 and 1.54 Å, respectively (the black vertical dotted lines in Fig. 3). The fractions of the distorted bond lengths (<1.42 Å) for the dense a-C film with the highest atomic density (4.0 g cm^{-3}, sp^3 content = 95.3%) and the H-added a-C film at maximum at% (31.2%, sp^3 content = 76.6%) were deduced separately, as shown in Table 1. The calculations for the Ref. a-C film were also obtained for comparison.

Table 1 Comparison of sp^3 content, fractions of the distorted bond, and bulk modulus in Ref. a-C, dense a-C, and H-added a-C films

	Ref. a-C	Dense a-C	H-added a-C
sp^3 content (%)	54.7	95.3	76.6
Fraction of distorted bond length (%)	17.2	1.0	14.3
Fraction of distorted bond angle (%)	35.8	15.6	33.1
Bulk modulus (GPa)	212	617	248

For the Ref. a-C film (Fig. 3), the fractions of the distorted bond length and bond angle are 17.2%, and 35.8%, respectively. For the dense a-C film, the fractions are 1.0% and 15.6%. However, after adding H into the a-C film, the fractions are 14.3% and 33.1%, showing similar values to both the bulk modulus and the fraction of the distorted bond length of the

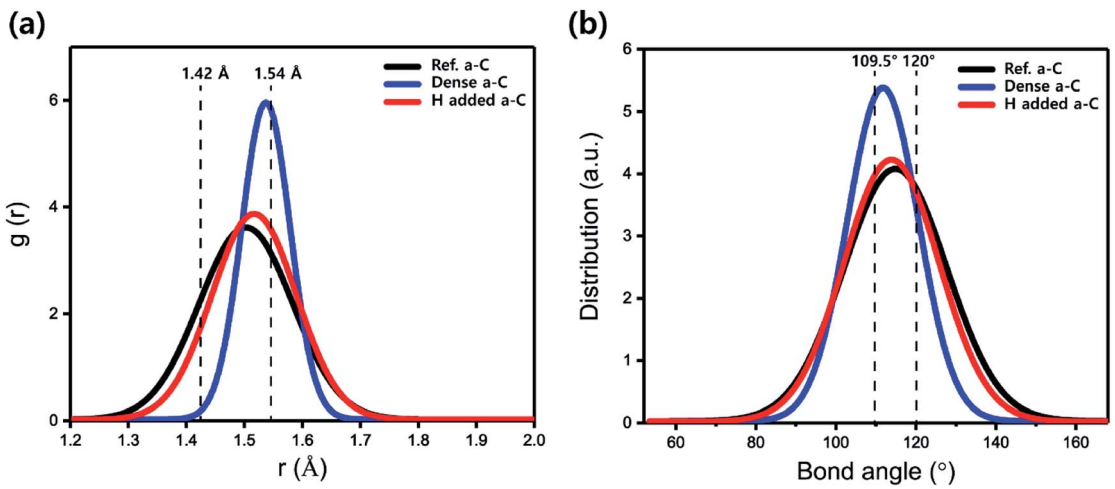

Fig. 3 (a) Bond length distributions and (b) bond angle distributions for Ref. a-C, dense a-C, and H-added a-C films, respectively.

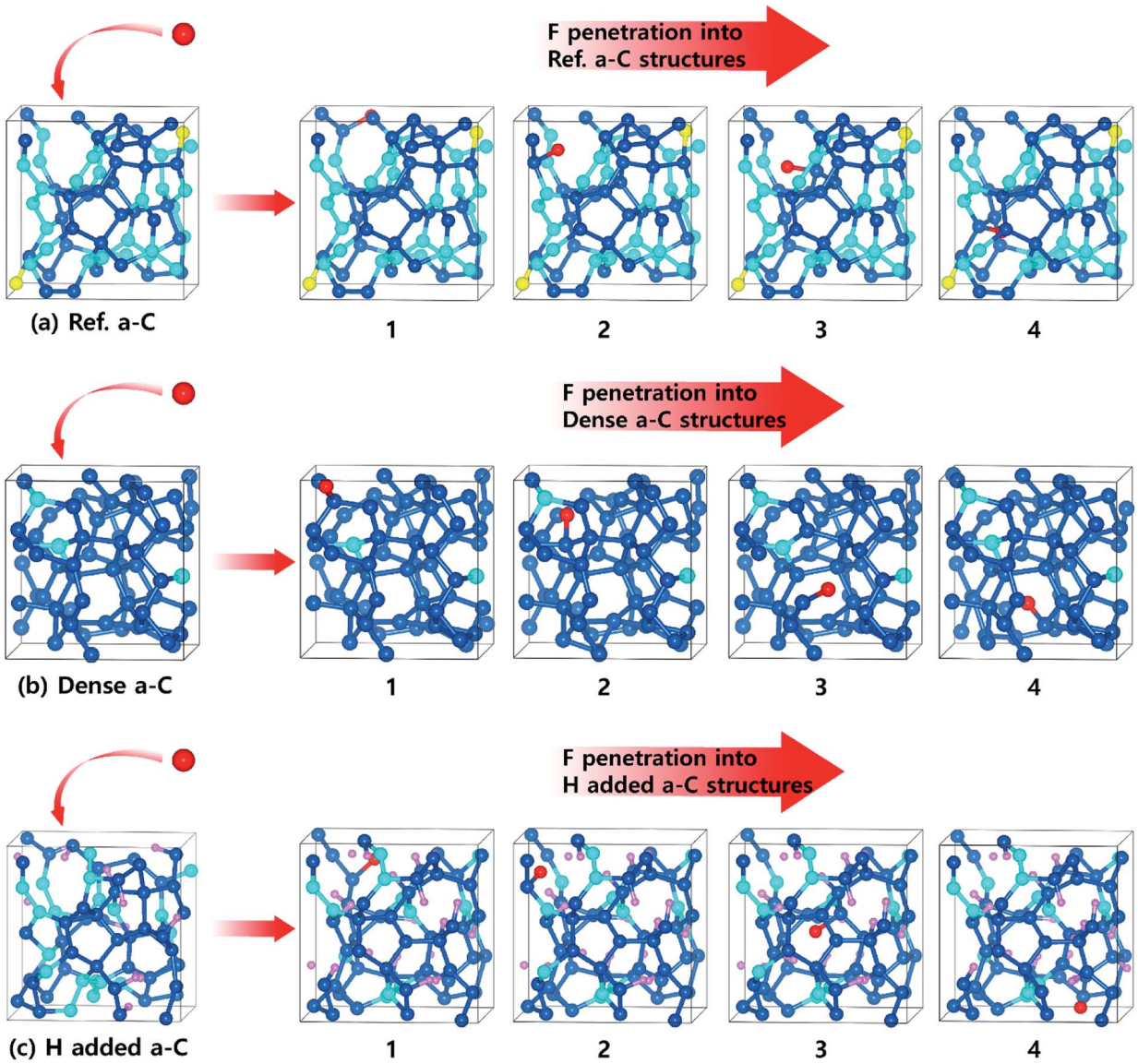

Fig. 4 The optimized structures of the first, second, third, and fourth states for the F penetration into the a-C films; (a) Ref. a-C, (b) dense a-C, and (c) H-added a-C films.

Ref. a-C film. This indicates that even the smaller bulk modulus than that of the dense a-C film is attributed to the high fraction of the distorted C–C bond relaxed by lattice vibrations during stress calculations using VASP.

So-Yeon Lee *et al.*,[40] reported that the RDF of the a-C films can be extracted from diffraction pattern measurements (mean bond length = 1.50 Å for the dense a-C film with sp^3 content = 78.5%; mean bond length = 1.45 Å for the normal a-C film with sp^3 content = 52.6%). These experimental RDF values show a similar trend with our DFT calculation results (mean bond length = 1.53 Å for the dense a-C film with sp^3 content = 95.3%; mean bond length = 1.50 Å for the Ref. a-C film with sp^3 content = 54.7%); however, there is slight discrepancy because the atoms in amorphous materials are bonded in randomly disordered positions due to the tendency that does not allow the formation of a regular atomic arrangement.

3.2. Influence of the atomic density and hydrogen concentration on diffusion profile of F atom in the point of energetics

During the dry etch process, the injection of etchant molecules such as CF_x leads to the penetration of F atoms through the a-C film up to the sub-layers. To enhance the performance of the a-C film as an etch hard mask, the a-C film has to block the F atoms on the top surface to diffuse downward up to the sub-layers, which are very important layers in highly integrated devices. For F diffusion to proceed, the F atom can pass though the dopant atom in the a-C films.

The optimized structures of the first, second, third, and fourth states for F penetration in the a-C films are shown in Fig. 4: (a) Ref. a-C film, (b) dense a-C film (at the highest density), (c) H-added a-C film (at the highest H concentration). Fig. 5 shows the minimum energy path of F diffusion,

corresponding to the 1st to 4th state in Fig. 4. The 1st state shows the energy profile of the downward diffusion of F atoms initially adsorbed on the top layer of the a-C films. In Fig. 4(a–c), Ref. and H-added a-C films show that the F atom diffuses downward and is bound to the sp^2 carbon atom.

Within the dense a-C film, the F atom diffuses downward and is bound to the surrounding carbon atom by breaking the C–C bond. The interesting point is that the F atom surrounded by sp^3 C atoms has much higher barriers compared to that for the Ref. a-C and H-added a-C films. This implies that the sp^2 C atoms play an important role in determining the diffusion path of the F atom because of the higher reactive nature of sp^2 C than that of sp^3 C.[19] Furthermore, in our previous study, we reported that the energy barrier for the diffusion of an F atom through the sp^3 bonding path is much higher than that for an F atom through the sp^2 boding path in a-C films.[40]

The energy diagram in Fig. 5 clearly shows that the dense a-C film has the highest energy barrier, which can be explained in two perspectives, that is, sp^3 content and atomic density. In the perspective of the sp^3 content, an increase in the sp^3 content causes the penetration of the F atom to weaken due to the decrease in the sp^2 carbon sites, enabling the formation of the C–F bonds and strengthening the blocking nature for F penetration. From the perspective of atomic density, an increase in the density leads to an increase in the sp^3 content and then hinders the diffusion of F atoms due to the surrounding dense sp^3 C atoms. Thus, the change in the sp^3 content by both atomic density and H concentration significantly impacts the blocking characteristic against the F atom.

3.3. Dynamic behaviors at finite temperatures

AIMD simulations were performed to examine the dynamic behavior of these three a-C structures. A simulation temperature of 1000 K was chosen. To better understand the dynamic properties, AIMD simulations were also performed to estimate the F mobility within these three a-C structures at 1000 K. The MD duration of 10 ps was used to calculate the mean-square displacements (MSD). Fig. 6 shows the variations in MSD as the simulation time progresses. The diffusion coefficients of F atoms can be calculated based on the Einstein relation:

$$D = \frac{\langle |R_i(t) - R_i(0)|^2 \rangle}{6t}$$

here, R_i is the atomic position; broken brackets denote thermal averages and t is the time.

For the Ref. a-C structure, the diffusion coefficient of F was predicted to be $D_F = 9.66 \times 10^{-4}$ cm^2 s^{-1}. The diffusivities of the dense and H-added a-C structures were estimated to be 2.22×10^{-4} and 4.83×10^{-4} cm^2 s^{-1}, respectively. These calculations clearly show that F mobility tends to be hindered by both the atomic density and H concentration. The drastic reduction in F diffusivities within the dense and H-added a-C structures can be explained by the enhancement in the characteristic barrier of F diffusion, as aforementioned in Section 3.2.

Table 2 shows the comparison of the sp^3 contents, activation energies (E_a, eV), and diffusion coefficients (D_F, cm^2 s^{-1}) for F diffusion for the Ref., dense, and H-added a-C films. This table clearly shows that the change in the sp^3 content by both atomic density and H concentration makes the diffusion barrier of the F atom even higher and suppresses the F diffusion, meaning that the F atom would follow the diffusion path passing through the sp^2 carbon and not the sp^3 carbon due to the significantly high barriers of 3.88 eV and 7.04 eV, respectively.

3.4. Discussion

According to several studies on the etch process,[41–43] during the initial etch process (within 10 s), etching is very fast because it has an unstable atomistic structure by dangling bonds of the top-surface atoms. However, after the initial etch of on the surface, the bulk part of the thin film starts to get slowly etched due to its characteristics of stable atomic bonds and condensed atomic arrangement. Due to this slow etching, the bulk etch process determines the overall etch reaction rate. Therefore, the reason we only considered the "bulk" part is that during the real

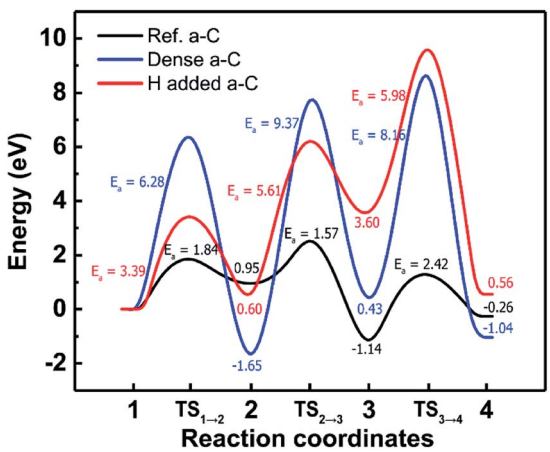

Fig. 5 Minimum energy path of F diffusion, corresponding to the initial, transition, and final states; Ref. a-C (black), dense a-C (blue), and H-added a-C (red) films. E_a means activation energy obtained from NEB calculations.

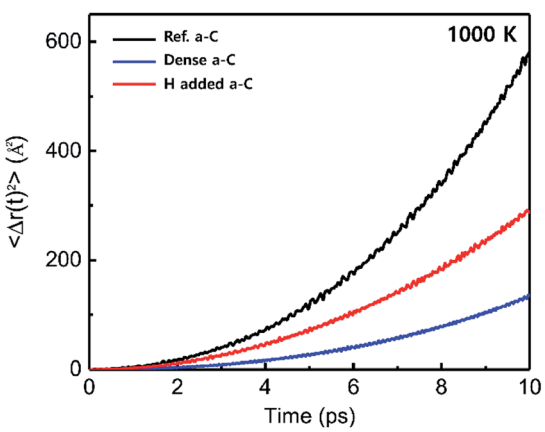

Fig. 6 Variations in the diffusivities of the F atom within the a-C films; Ref. a-C (black), dense a-C (blue), and H-added a-C (red) films.

Table 2 Comparison of sp^3 content, activation energies (E_a, eV), and diffusion coefficients (D_F, $cm^2\ s^{-1}$) for F diffusion on Ref., dense, and H-added a-C films

	Ref. a-C	Dense a-C	H-added a-C
sp^3 content (%)	54.7	95.3	76.6
$E_{a,min}$ (eV)	1.57	3.39	6.28
$E_{a,max}$ (eV)	2.42	5.98	9.37
D_F ($cm^2\ s^{-1}$)	9.66	2.22	4.83

etch process, the "surface" part takes place in a very short time and most of the time is required for the "bulk" part. In fact, many other researchers in the fields of etch processes[44–46] have controlled the etch profile by tuning the "density" of thin films, which is a very important "bulk" property that can be easily tuned by the etch chemistry ratio, temperature, and plasma power.

Our DFT calculation shows that increasing the atomic density of the a-C films dramatically increases the bulk modulus. Similarly, several researchers reported experimentally that the bulk modulus of a-C is proportional to density.[12,47–49] Ito A. M. *et al.*[49] explained the dependence of the bulk modulus on density by counting the covalent bonds in a-C materials. They revealed that the number of covalent bonds increased in proportion to the film density as well as the bulk modulus. Other researchers[50,51] stated that an increase in the modulus is attributed to the change from sp^2 to sp^3 bonds with an increase in the density. The combination of their results and our DFT calculated results for the relation between density and bulk modulus in actual thin films provides deep insights for analyzing the thin film chemistry and physics from this approach.

All our DFT calculated results suggest that the dense a-C film would be difficult to apply for highly integrated devices due to the high bulk modulus even though this film has a superior F blocking nature. On the other hand, the H-added a-C film would have an advantage for highly integrated devices due to the excellent F blocking nature by keeping the bulk modulus from rising steeply.

Even though a-C films with increasing atomic density and H concentration have not been reported as an etch hard mask, our DFT calculated results suggest that the H-added a-C films would have outstanding characteristics such as mechanical properties and blocking nature of F atoms for an etch hard mask in ultra-high integrated semiconductor devices. In our DFT calculated results, the combinational study of atomic density and H concentration in the a-C films would provide a deep insight into improving the mechanical properties and etch selectivity of the films, enhancing the performance of the future memory devices.

4. Conclusions

We investigated the energetics, structure, and mechanical properties of a-C films with an increase in the sp^3 content by adjusting the atomic density or hydrogen content based on DFT and AIMD calculations. Drastic increase in bulk modulus was observed by increasing the atomic density of the a-C films, which suggested that it would be difficult for the films hardened by high atomic density to relieve the stress of the individual layers within the overall stack in integrated semiconductor devices. However, the addition of hydrogen into the a-C films had little effect on increasing the bulk modulus even though the sp^3 content increased. These findings suggest that the process design for high-sp^3-content a-C films should be carried out by adding hydrogen rather than increasing atomic density. These requirements become more important and increasingly challenging to meet as the device integrity increases. In the perspective of the F blocking nature, a change in the sp^3 content by both atomic density and H concentration makes the diffusion barrier of the F atom even higher and suppresses the F diffusion, meaning that the F atom would follow the diffusion path that passes the sp^2 carbon and not the sp^3 carbon due to the significantly high barrier. For the material design of a-C films with adequate doped characteristics, our results can provide a new straightforward strategy to tailor the a-C films with excellent mechanical and other novel physical and chemical properties.

Conflicts of interest

There are no conflicts to declare.

Acknowledgements

Euijoon Yoon and Gun-Do Lee acknowledge support from the Supercomputing Center/Korea Institute of Science and Technology Information with supercomputing resources (KSC-2017-C3-0020), from the joint program for Samsung Electronics Co., Ltd. (SEC), from BK21PLUS SNU Materials Division for Educating Creative Global Leaders (21A20131912052), and from the National Research Foundation of Korea (NRF) grant funded by the Korea government (No. RIAM 2019R1A2C2005098) and the Ministry of Science, ICT and Future Planning (2017M3D1A1040688). Hwanyeol Park acknowledge support from the Supercomputing Center/Korea Institute of Science and Technology Information with supercomputing resources (KSC-2019-CRE-0148). The computation data to support the findings of this paper is available from the corresponding author on reasonable request. The code to analyze *ab initio* molecular dynamics simulation is available at: https://github.com/mogroupumd/aimd.

References

1 J. Robertson, Diamond-like amorphous carbon, *Mater. Sci. Eng. R Rep.*, 2002, **37**(4–6), 129–281.
2 L. Zhang, X. Wei, Y. Lin and F. Wang, A ternary phase diagram for amorphous carbon, *Carbon*, 2015, **94**, 202–213.
3 L. Wang, R. Zhang, U. Jansson and N. Nedfors, A near-wearless and extremely long lifetime amorphous carbon film under high vacuum, *Sci. Rep.*, 2015, **5**, 11119.

4 X. Li, P. Guo, L. Sun, A. Wang and P. Ke, Ab Initio Investigation on Cu/Cr Codoped Amorphous Carbon Nanocomposite Films with Giant Residual Stress Reduction, *ACS Appl. Mater. Interfaces*, 2015, **7**, 27878–27884.

5 G. Cicala, P. Bruno and A. M. Losacco, PECVD of hydrogenated diamond-like carbon films from CH_4–Ar mixtures: growth chemistry and material characteristics, *Diamond Relat. Mater.*, 2004, **13**, 1361–1365.

6 Y. T. Kim, S. M. Cho, W. S. Choi, B. Hong and D. H. Yoon, Dependence of the bonding structure of DLC thin films on the deposition conditions of PECVD method, *Surf. Coat. Technol.*, 2003, **169–170**, 291–294.

7 H. Yang, G. A. Brown, J. C. Hu, J. P. Lu, R. Kraft, A. L. P. Rotondaro, S. V. Hattangady, I. Chen, J. D. Luttmer, R. A. Chapman, P. J. Chen, H. L. Tsai, B. Amirhekmat and L. K. Magel, A comparison of TiN processes for CVD W/TiN gate electrode on 3 nm gate oxide, in *International Electron Devices Meeting*, IEDM Technical Digest, 1997, pp. 459–462.

8 M. Dammann, M. Chertouk, W. Jantz, K. Köhler and G. Weimann, Reliability of InAlAs/InGaAs HEMTs grown on GaAs substrate with metamorphic buffer, *Microelectron. Reliab.*, 2000, **40**, 1709–1713.

9 J. Robertson, Electronic and atomic structure of diamond-like carbon, *Semicond. Sci. Technol.*, 2003, **18**, S12–S19.

10 N. Maître, S. Camelio, A. Barranco, T. Girardeau and E. Breelle, Physical and chemical properties of amorphous hydrogenated carbon films deposited by PECVD in a low self-bias range, *J. Non-Cryst. Solids*, 2005, **351**, 877–884.

11 N. Fourches and G. Turban, Plasma deposition of hydrogenated amorphous carbon: growth rates, properties and structures, *Thin Solid Films*, 1994, **240**, 28–38.

12 J. Robertson, Diamond-like amorphous carbon, *Mater. Sci. Eng., R*, 2002, **37**, 129–281.

13 T. Mikami, H. Nakazawa, M. Kudo and M. Mashita, Effects of hydrogen on film properties of diamond-like carbon films prepared by reactive radio-frequency magnetron sputtering using hydrogen gas, *Thin Solid Films*, 2005, **488**, 87–92.

14 E. Vietzke, K. Flaskamp, V. Philipps, G. Esser, P. Wienhold and J. Winter, Chemical erosion of amorphous hydrogenated carbon films by atomic and energetic hydrogen, *J. Nucl. Mater.*, 1987, **145–147**, 443–447.

15 C. Wei, K.-S. Peng and M.-S. Hung, The effect of hydrogen and acetylene mixing ratios on the surface, mechanical and biocompatible properties of diamond-like carbon films, *Diamond Relat. Mater.*, 2016, **63**, 108–114.

16 M. Silinskas, A. Grigonis, V. Kulikauskas and I. Manika, Hydrogen influence on the structure and properties of amorphous hydrogenated carbon films deposited by direct ion beam, *Thin Solid Films*, 2008, **516**, 1683–1692.

17 R.-h. Zhang, L.-p. Wang and Z.-b. Lu, Probing the intrinsic failure mechanism of fluorinated amorphous carbon film based on the first-principles calculations, *Sci. Rep.*, 2015, **5**, 9419.

18 X. Li, P. Ke and A. Wang, Probing the Stress Reduction Mechanism of Diamond-Like Carbon Films by Incorporating Ti, Cr, or W Carbide-Forming Metals: Ab Initio Molecular Dynamics Simulation, *J. Phys. Chem. C*, 2015, **119**, 6086–6093.

19 H. Park, S. Lee, H. J. Kim, D. Woo, S. J. Park, J. M. Lee, E. Yoon and G.-D. Lee, Effects of nitrogen doping in amorphous carbon layers on the diffusion of fluorine atoms: a first-principles study, *J. Appl. Phys.*, 2019, **125**, 155701.

20 R. Haerle, A. Pasquarello and A. Baldereschi, First-principle study of C 1s core-level shifts in amorphous carbon, *Comput. Mater. Sci.*, 2001, **22**, 67–72.

21 R. Haerle, E. Riedo, A. Pasquarello and A. Baldereschi, sp^2/sp^3 hybridization ratio in amorphous carbon from C 1s core-level shifts: X-ray photoelectron spectroscopy and first-principles calculation, *Phys. Rev. B: Condens. Matter Mater. Phys.*, 2001, **65**, 045101.

22 H. Park, D. Woo, J. M. Lee, S. J. Park, S. Lee, H. J. Kim, E. Yoon and G.-D. Lee, First principles investigation on energetics, structure, and mechanical properties of amorphous carbon films doped with B, N, and Cl, *Sci. Rep.*, 2019, **9**, 18961.

23 J. P. Perdew, K. Burke and M. Ernzerhof, Generalized gradient approximation made simple, *Phys. Rev. Lett.*, 1996, **77**, 3865–3868.

24 G. Kresse and J. Furthmuller, Efficient iterative schemes for ab initio total-energy calculations using a plane-wave basis set, *Phys. Rev. B: Condens. Matter Mater. Phys.*, 1996, **54**, 11169–11186.

25 S. Grimme, Semiempirical GGA-type density functional constructed with a long-range dispersion correction, *J. Comput. Chem.*, 2006, **27**, 1787–1799.

26 P. E. Blöchl, Projector augmented-wave method, *Phys. Rev. B: Condens. Matter Mater. Phys.*, 1994, **50**, 17953–17979.

27 W. Zhai, X. Song, T. Li, B. Yu, W. Lu and K. Zeng, Ti Reactive Sintering of Electrically Conductive Al_2O_3–TiN Composite: Influence of Ti Particle Size and Morphology on Electrical and Mechanical Properties, *Materials*, 2017, **10**, 1348.

28 D. Vanderbilt, Soft self-consistent pseudopotentials in a generalized eigenvalue formalism, *Phys. Rev. B: Condens. Matter Mater. Phys.*, 1990, **41**, 7892–7895.

29 G. Henkelman, B. P. Uberuaga and H. Jónsson, A climbing image nudged elastic band method for finding saddle points and minimum energy paths, *J. Chem. Phys.*, 2000, **113**, 9901–9904.

30 G. Mills and H. Jónsson, Quantum and thermal effects in ${\mathrm{H}}_{2}$ dissociative adsorption: evaluation of free energy barriers in multidimensional quantum systems, *Phys. Rev. Lett.*, 1994, **72**, 1124–1127.

31 D. R. Alfonso and K. D. Jordan, A flexible nudged elastic band program for optimization of minimum energy pathways using ab initio electronic structure methods, *J. Comput. Chem.*, 2003, **24**, 990–996.

32 H. Park, S. Lee, H. J. Kim, E. Yoon and G.-D. Lee, Dissociation reaction of B_2H_6 on TiN surfaces during atomic layer deposition: first-principles study, *RSC Adv.*, 2017, **7**, 55750–55755.

33 H. Park, S. Lee, H. J. Kim, D. Woo, S. J. Park, K. Kim, E. Yoon and G.-D. Lee, Effects of H_2 and N_2 treatment for B_2H_6

dosing process on TiN surfaces during atomic layer deposition: an ab initio study, *RSC Adv.*, 2018, **8**, 21164–21173.

34 H. Park, S. Lee, H. J. Kim, D. Woo, J. M. Lee, E. Yoon and G.-D. Lee, Overall reaction mechanism for a full atomic layer deposition cycle of W films on TiN surfaces: first-principles study, *RSC Adv.*, 2018, **8**, 39039–39046.

35 H. Park, E. Yoon, G.-D. Lee and H. J. Kim, Analysis of surface adsorption kinetics of SiH_4 and Si_2H_6 for deposition of a hydrogenated silicon thin film using intermediate pressure SiH_4 plasmas, *Appl. Surf. Sci.*, 2019, **496**, 143728.

36 I. N. Remediakis, M. G. Fyta, C. Mathioudakis, G. Kopidakis and P. C. Kelires, Structure, elastic properties and strength of amorphous and nanocomposite carbon, *Diamond Relat. Mater.*, 2007, **16**, 1835–1840.

37 H. Ito, M. Kuwahara, R. Ohta and M. Usui, Behavior of stress generated in semiconductor chips with high-temperature joints: influence of mechanical properties of joint materials, *J. Appl. Phys.*, 2018, **123**, 145109.

38 M. Koganemaru, K. Yoshida, T. Ikeda, N. Miyazaki and H. Tomokage, Device simulation for evaluating effects of mechanical stress on semiconductor devices: impact of stress-induced variation of electron effective mass, in *3rd Electronics System Integration Technology Conference ESTC*, 2010, pp. 1–6.

39 X. Li, P. Ke, H. Zheng and A. Wang, Structural properties and growth evolution of diamond-like carbon films with different incident energies: a molecular dynamics study, *Appl. Surf. Sci.*, 2013, **273**, 670–675.

40 S.-Y. Lee, K.-T. Jang, M.-W. Jeong, S. Kim, H. Park, K. Kim, G.-D. Lee, M. Kim and Y.-C. Joo, Bonding structure and etching characteristics of amorphous carbon for a hardmask deposited by DC sputtering, *Carbon*, 2019, **154**, 277–284.

41 H. Zhu, J. Hüpkes, E. Bunte, J. Owen and S. M. Huang, Novel etching method on high rate ZnO:Al thin films reactively sputtered from dual tube metallic targets for silicon-based solar cells, *Sol. Energy Mater. Sol. Cells*, 2011, **95**, 964–968.

42 D. H. van Dorp, S. Arnauts, F. Holsteyns and S. De Gendt, Wet-Chemical Approaches for Atomic Layer Etching of Semiconductors: Surface Chemistry, Oxide Removal and Reoxidation of InAs (100), *ECS J. Solid State Sci. Technol.*, 2015, **4**, N5061–N5066.

43 J. Provine, P. Schindler, Y. Kim, S. P. Walch, H. J. Kim, K.-H. Kim and F. B. Prinz, Correlation of film density and wet etch rate in hydrofluoric acid of plasma enhanced atomic layer deposited silicon nitride, *AIP Adv.*, 2016, **6**, 065012–0650128.

44 Z. Ming, X. De Yuan, P. S. Min, H. Z. Shan and S. Y. Xie, Experimental study of multilayer SiCN barrier film in 45/40 nm technological node and beyond, *Microelectron. Reliab.*, 2016, **57**, 86–92.

45 T.-S. Choi and D. W. Hess, Chemical Etching and Patterning of Copper, Silver, and Gold Films at Low Temperatures, *ECS J. Solid State Sci. Technol.*, 2014, **4**, N3084–N3093.

46 N. Kuboi, T. Tatsumi, H. Minari, M. Fukasawa, Y. Zaizen, J. Komachi and T. Kawamura, Influence of hydrogen in silicon nitride films on the surface reactions during hydrofluorocarbon plasma etching, *J. Vac. Sci. Technol., A*, 2017, **35**, 061306.

47 J. Robertson, Deposition mechanisms for promoting sp^3 bonding in diamond-like carbon, *Diamond Relat. Mater.*, 1993, **2**, 984–989.

48 P. J. Fallon, V. S. Veerasamy, C. A. Davis, J. Robertson, G. A. J. Amaratunga, W. I. Milne and J. Koskinen, Properties of filtered-ion-beam-deposited diamondlike carbon as a function of ion energy, *Phys. Rev. B: Condens. Matter Mater. Phys.*, 1993, **48**, 4777–4782.

49 A. M. Ito, A. Takayama, Y. Oda and H. Nakamura, The first principle calculation of bulk modulus and Young's modulus for amorphous carbon material, *J. Phys.: Conf. Ser.*, 2014, **518**, 012011.

50 A. C. Ferrari, B. Kleinsorge, N. A. Morrison, A. Hart, V. Stolojan and J. Robertson, Stress reduction and bond stability during thermal annealing of tetrahedral amorphous carbon, *J. Appl. Phys.*, 1999, **85**, 7191–7197.

51 J. Robertson, Mechanical properties and coordinations of amorphous carbons, *Phys. Rev. Lett.*, 1992, **68**, 220–223.

